# Measurement and resonance analysis of the 33S(n, α)30Si cross section at the CERN n_TOF facility in the energy region from 10 to 300 keV

**Praena, J.; ...; Bosnar, Damir; ...; Žugec, Petar**

# Measurement and resonance analysis of the $^{33}S(n,\alpha)^{30}Si$ cross section at the CERN n_TOF facility in the energy region from 10 to 300 keV

J. Praena,[1,*] M. Sabaté-Gilarte,[2,3] I. Porras,[1] J. M. Quesada,[2] S. Altstadt,[4] J. Andrzejewski,[5] L. Audouin,[6] V. Bécares,[7] M. Barbagallo,[8] F. Bečvář,[9] F. Belloni,[10] E. Berthoumieux,[10] J. Billowes,[11] V. Boccone,[3] D. Bosnar,[12] M. Brugger,[3] F. Calviño,[13] M. Calviani,[3] D. Cano-Ott,[7] C. Carrapiço,[14] F. Cerutti,[3] E. Chiaveri,[3,10] M. Chin,[3] N. Colonna,[8] G. Cortés,[13] M. A. Cortés-Giraldo,[2] M. Diakaki,[15] M. Dietz,[16] C. Domingo-Pardo,[17] R. Dressler,[18] I. Durán,[19] C. Eleftheriadis,[20] A. Ferrari,[3] K. Fraval,[10] V. Furman,[21] K. Göbel,[4] M. B. Gómez-Hornillos,[13] S. Ganesan,[22] A. R. García,[7] G. Giubrone,[17] I. F. Gonçalves,[14] E. González-Romero,[7] A. Goverdovski,[23] E. Griesmayer,[24] C. Guerrero,[2,3] F. Gunsing,[10] T. Heftrich,[4] A. Hernández-Prieto,[3,13] J. Heyse,[25] D. G. Jenkins,[26] E. Jericha,[24] F. Käppeler,[27] Y. Kadi,[3] D. Karadimos,[15] T. Katabuchi,[28] V. Ketlerov,[23] V. Khryachkov,[23] N. Kivel,[18] P. Koehler,[29] M. Kokkoris,[15] J. Kroll,[9] M. Krtička,[9] C. Lampoudis,[10] C. Langer,[4] E. Leal-Cidoncha,[19] C. Lederer-Woods,[16] H. Leeb,[24] L. S. Leong,[6] J. Lerendegui-Marco,[2] R. Losito,[3] A. Mallick,[22] A. Manousos,[20] J. Marganiec,[5] T. Martínez,[7] C. Massimi,[30,31] P. Mastinu,[32] M. Mastromarco,[8] E. Mendoza,[7] A. Mengoni,[33] P. M. Milazzo,[34] F. Mingrone,[30] M. Mirea,[35] W. Mondelaers,[25] C. Paradela,[19] A. Pavlik,[36] J. Perkowski,[5] A. J. M. Plompen,[25] T. Rauscher,[37] R. Reifarth,[4] A. Riego-Perez,[13] M. Robles,[19] C. Rubbia,[3] J. A. Ryan,[11] R. Sarmento,[14] A. Saxena,[22] P. Schillebeeckx,[25] S. Schmidt,[4] D. Schumann,[18] P. Sedyshev,[21] G. Tagliente,[8] J. L. Tain,[17] A. Tarifeño-Saldivia,[17] D. Tarrío,[19] L. Tassan-Got,[6] A. Tsinganis,[3] S. Valenta,[9] G. Vannini,[30,31] V. Variale,[8] P. Vaz,[14] A. Ventura,[30] M. J. Vermeulen,[26] V. Vlachoudis,[3] R. Vlastou,[15] A. Wallner,[38] T. Ware,[11] M. Weigand,[4] C. Weiss,[24] T. Wright,[11] and P. Žugec[12]
(n_TOF Collaboration)

[1]*Universidad de Granada, Granada, Spain*
[2]*Universidad de Sevilla, Seville, Spain*
[3]*European Organization for Nuclear Research (CERN), Geneva, Switzerland*
[4]*Goethe University Frankfurt, Frankfurt, Germany*
[5]*University of Lodz, Lodz, Poland*
[6]*Institut de Physique Nucléaire, CNRS-IN2P3, Univesité Paris-Sud, Université Paris-Saclay, F-91406 Orsay Cedex, France*
[7]*Centro de Investigaciones Energéticas Medioambientales y Tecnológicas (CIEMAT), Madrid, Spain*
[8]*Istituto Nazionale di Fisica Nucleare, Sezione di Bari, Bari, Italy*
[9]*Charles University, Prague, Czech Republic*
[10]*CEA Irfu, Université Paris-Saclay, F-91191 Gif-sur-Yvette, France*
[11]*University of Manchester, Manchester, United Kingdom*
[12]*Department of Physics, Faculty of Science, University of Zagreb, Zagreb, Croatia*
[13]*Universitat Politècnica de Catalunya, Barcelona, Spain*
[14]*Instituto Superior Técnico, Lisbon, Portugal*
[15]*National Technical University of Athens, Athens, Greece*
[16]*School of Physics and Astronomy, University of Edinburgh, Edinburgh, United Kingdom*
[17]*Instituto de Física Corpuscular, CSIC-Universidad de Valencia, Spain*
[18]*Paul Scherrer Institut (PSI), Villingen, Switzerland*
[19]*University of Santiago de Compostela, Santiago de Compostela, Spain*
[20]*Aristotle University of Thessaloniki, Thessaloniki, Greece*
[21]*Joint Institute for Nuclear Research (JINR), Dubna, Russia*
[22]*Bhabha Atomic Research Centre (BARC), Mumbai, India*
[23]*Institute of Physics and Power Engineering (IPPE), Obninsk, Russia*
[24]*Technische Universität Wien, Wien, Austria*
[25]*European Commission, Joint Research Centre, Geel, Retieseweg 111, B-2440 Geel, Belgium*
[26]*University of York, York, United Kingdom*
[27]*Karlsruhe Institute of Technology, Campus North, IKP, 76021 Karlsruhe, Germany*
[28]*Tokyo Institute of Technology, Tokyo, Japan*
[29]*Oak Ridge National Laboratory (ORNL), Oak Ridge, Tennessee 37831, USA*

[*]jpraena@ugr.es

[30]*Istituto Nazionale di Fisica Nucleare, Sezione di Bologna, Bologna, Italy*
[31]*Dipartimento di Fisica e Astronomia, Università di Bologna, Bologna, Italy*
[32]*Istituto Nazionale di Fisica Nucleare, Sezione di Legnaro, Legnaro, Italy*
[33]*Agenzia Nazionale per le Nuove Tecnologie (ENEA), Bologna, Italy*
[34]*Istituto Nazionale di Fisica Nucleare, Sezione di Trieste, Trieste, Italy*
[35]*Horia Hulubei National Institute of Physics and Nuclear Engineering, Măgurele, Romania*
[36]*University of Vienna, Faculty of Physics, Vienna, Austria*
[37]*Department of Physics, University of Basel, Basel, Switzerland*
[38]*Australian National University, Canberra, Australia*

(Received 11 April 2018; revised manuscript received 9 May 2018; published 4 June 2018)

The $^{33}$S$(n,\alpha)^{30}$Si cross section has been measured at the neutron time-of-flight (n_TOF) facility at CERN in the neutron energy range from 10 to 300 keV relative to the $^{10}$B$(n,\alpha)^{7}$Li cross-section standard. Both reactions were measured simultaneously with a set of micromegas detectors. The flight path of 185 m has allowed us to obtain the cross section with high-energy resolution. An accurate description of the resonances has been performed by means of the multilevel multichannel $R$-matrix code SAMMY. The results show a significantly higher area of the biggest resonance (13.45 keV) than the unique high-resolution $(n,\alpha)$ measurement. The new parametrization of the 13.45-keV resonance is similar to that of the unique transmission measurement. This resonance is a matter of research in neutron-capture therapy. The $^{33}$S$(n,\alpha)^{30}$Si cross section has been studied in previous works because of its role in the production of $^{36}$S in stars, which is currently overproduced in stellar models compared to observations.

DOI: 10.1103/PhysRevC.97.064603

## I. INTRODUCTION

The $^{33}$S$(n,\alpha)^{30}$Si reaction combines simultaneously the properties of a low-mass stable isotope with a high-$Q$ value (3.5 MeV) for neutron-induced ion emission and a high cross-section due to the resonances present in the keV region. These interesting properties were pointed out in Ref. [1] for its possible application to radiotherapy with neutrons and a specific target inserted in the tumor tissue. This technique is known as BNCT (boron neutron-capture therapy) because $^{10}$B has been so far the target for neutrons in the experimental treatments of tumors, all of them performed at nuclear reactors [2]. Forthcoming accelerator-based neutron-capture therapy facilities will deliver neutrons in the epithermal energy range (a few killoelectron volts); therefore such neutron beams could also deliver a significant dose in the first centimeters of tissue, before the neutrons are thermalized, if an adequate compound containing $^{33}$S is absorbed in the tissue. The conceptual use of $^{33}$S in BNCT for superficial tumors or tumors growing towards the skin was studied with the simulation of the dose transferred to ICRU tissue [3,4].

One of the key points for a reliable simulation of the dose delivered by the $^{33}$S$(n,\alpha)^{30}$Si reaction, and consequently its possible use in BNCT with epithermal neutron beams, is the value of the cross section at the first and most important resonance (at $E_n = 13.45$ keV) or equivalently its description by means of resonance parameters. There are only two available measurements describing the cross section in terms of resonance parameters: the transmission experiment performed by Coddens *et al.* at ORELA [5] and the $(n,\alpha)$ measurement of Wagemans *et al.* at GELINA [6]. Both works combined their data and analysis; however, among others, the two data sets showed an important discrepancy: the transmission measurement provided a value of the $\alpha$ width $(\Gamma_\alpha)$ of the 13.45-keV resonance that is twice the value deduced from $(n,\alpha)$ measurement as it was pointed out in both works [5,6]. The experiment performed at n_TOF aims at clarifying this discrepancy. In addition, a complete description of the cross section making use of the SAMMY code [7] will be provided.

Concerning the evaluated data, the main databases do not show a resonance structure. In addition, there are two different energy dependencies adopted for this cross section in the evaluations, which do not match the scarce experimental data: a constant value above thermal (i.e., ENDF/B-VII.1) and a $1/\sqrt{E}$ behavior between thermal and 5 keV followed by a rapid increase of the cross section up to 30 keV (i.e., JEFF-3.2). EAF-2010 is the only database showing a resonance structure but with huge discrepancies with the available experimental data [8].

The interest in the possible use of $^{33}$S in BNCT is quite recent. In fact, the research carried out on $^{33}$S$(n,\alpha)^{30}$Si has originally been linked to nuclear astrophysics due to its role in the origin of the neutron-rich isotope $^{36}$S, which remains an open question. The experimental results of Wagemans *et al.* [6] and Auchampaugh *et al.* [9] were applied to explosive scenarios showing a $^{36}$S overproduction in the solar system incompatible with the stellar models. Later, the $s$-process contribution to the total $^{36}$S abundance was drastically reduced by the $^{34}$S$(n,\gamma)$ reaction, which acts as a bottleneck because of its very low stellar cross-section [10].

The present work describes the measurement of the $^{33}$S$(n,\alpha)^{30}$S cross section at the n_TOF facility at CERN in the energy range from 10 to 300 keV. A detailed $R$-matrix resonance analysis has been carried out to provide more accurate data for future applications in BNCT and astrophysics.

## II. EXPERIMENTAL SETUP

### A. The n_TOF neutron beam at EAR1

The experiment was performed in the experimental area 1 (EAR1) of the n_TOF facility at CERN, located 185 m from the neutron production target. The neutrons are generated by the 20 GeV/$c$ proton beam from the CERN PS (proton synchrotron) impinging on a lead target. The measurement was performed with a cooling-moderation configuration consisting of demineralized water and borated water. The technical features of the facility and the characteristics of the neutron beam are described in detail in Refs. [11,12]. Concerning the $^{33}$S$(n,\alpha)^{30}$Si measurement, the most important characteristics of the beam are the high resolution in neutron energy for an accurate description of the resonances and the large aperture of the beam, 8 cm in diameter, which allows the use of large thin samples increasing the expected low-count rate. The use of borated water as moderator minimizes neutron capture on hydrogen, and hence the associated in-beam $\gamma$-ray background in neutron-capture cross-section measurements. The most important consequence for this measurement is a strong reduction of the thermal peak in the neutron flux.

### B. The samples

The production of thin sulfur samples is difficult because sulfur adheres poorly to most materials and sublimates at room temperature in a vacuum [6,9,13]. Previous experiments reported problems related to $^{33}$S loss [6,9]. Six $^{33}$S samples were prepared by the vacuum surface coatings (VSC) group of the Technology Department at CERN. The method developed for coating the samples was based on the thermal evaporation of $^{33}$S powder on dedicated copper-plated Kapton foils to form a stable compound. Samples 8 cm in diameter were produced in order to take advantage of the largest neutron beam spot and the highest fluence at EAR1 during the so-called fission campaign. The characterization of the samples was carried out by means of Rutherford backscattering spectrometry (RBS) at the Centro Nacional de Aceleradores (Spain) [14]. With this technique it is possible to achieve a precise determination of the number of atoms with low uncertainty. A monoenergetic beam of 3.5-MeV $^4$He$^{++}$ ions was used and each sample was scanned from one edge to the other passing through the center. Several RBS measurements and analyses were performed before and after the experiment, and the conclusion was that no sulfur was lost under high vacuum or in contact with different gases at atmospheric pressure; therefore, the samples showed an excellent adherence and stability. A detailed discussion on the preparation and characterization of the samples can be found in Ref. [15]. Table I summarizes the results for all the samples.

The $^{10}$B$(n,\alpha)^7$Li cross-section standard was use as reference in the present measurement. Differently from the $^{33}$S sample, the production of $^{10}$B$_4$C samples is done routinely in different labs. The $^{10}$B$_4$C sample used was also prepared by the VSC group by dc magnetron sputtering. It was 8 cm in diameter and it was irradiated in parallel with the $^{33}$S samples. The thickness was determined by scanning electron microscopy (SEM), giving a value of $(8.1 \pm 0.2) \times 10^{-6}$ atoms of $^{10}$B atoms per barn.

### C. Detector and acquisition

The measurement was performed with a micropattern gaseous detector based on microbulk technology known as micro mesh gaseous structure (Micromegas) [16]. The low-mass, robustness, and neutron and $\gamma$ transparency of this technology permit the use of several in-beam detectors with a minimal perturbation of the neutron beam [17]. The geometrical efficiency is close to 50% if only one of the two reaction products is detected, as was the case in the present experiment. This kind of detector has been extensively used at n_TOF, for instance, for monitoring purposes and flux determination [12].

The reaction chamber housed nine Micromegas (MGAS) detectors for six $^{33}$S samples, two blank samples for background studies, all of them in back-to-back configuration, and one $^{10}$B reference sample. In this way, systematic and statistical uncertainties could be reduced. A blank sample is the substrate of a $^{33}$S sample, copper-plated Kapton foil. The experiment was carried out in the usual configuration of MGAS at n_TOF [12], in which the electrons from the ionization of the gas (88% Ar, 10% $CF_4$, 2% $iC_4H_{10}$) at atmospheric pressure are collected and the multiplication works as internal gain but with no amplification of the electronic noise, ensuring a good signal-to-noise ratio.

The signals from the MGAS were directly processed with the standard n_TOF data acquisition system (DAQ) [18] based on flash ADCs with a sampling rate up to 2 gigasamples per second, 12 bit resolution, and 8 MBytes on-board memory. For all detectors, the data were recorded for a time-of-flight up to 50 ms, corresponding to nearly thermal neutron energy; however, no data have been obtained below 10 keV in the present experiment. The starting signal for determining the time-of-flight of the neutrons was given by the prompt $\gamma$-flash generated in the interaction of the 20 GeV/$c$ proton beam with the lead target.

## III. DATA ANALYSIS

The signals from each MGAS detector were analyzed off-line with a routine that extracted the baseline, the amplitude, and the time of flight (TOF). Figure 1 shows a scatter plot of the pulse height of the signals versus their TOF for a detector facing a $^{33}$S sample. Few structures are resolved, and the signals due to $\alpha$ particles are clearly above the noise and background. For instance, the two structures around a flight time of $10^5$ ns correspond to resonances at 23.95 and 13.45 keV.

TABLE I. Areal density of the $^{33}$S samples in number of atoms per barn [15].

| | Areal density (atoms/b) $\times 10^{-7}$ |
|---|---|
| Sample 1 | $3.79 \pm 0.31$ |
| Sample 2 | $3.49 \pm 0.28$ |
| Sample 3 | $2.59 \pm 0.23$ |
| Sample 4 | $2.15 \pm 0.20$ |
| Sample 5 | $3.76 \pm 0.31$ |
| Sample 6 | $3.65 \pm 0.29$ |

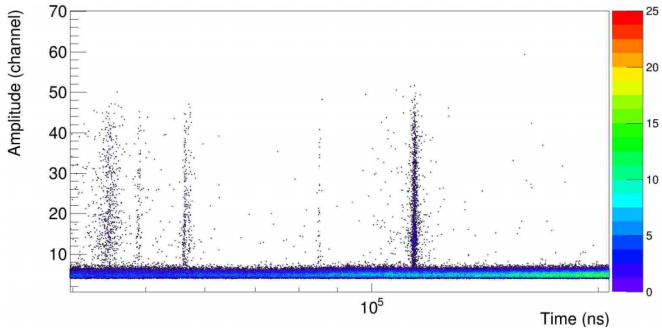


FIG. 1. Scatter plot of the signal amplitude in arbitrary units (channels) versus TOF for a $^{33}$S sample.

As mentioned before, to study the background due to the backing of the sample, two MGAS detectors were dedicated to record the signals coming from two blank samples (no $^{33}$S). Figure 2 shows the scatter plot of the pulse height versus TOF for a blank sample. The comparison between Figs. 1 and 2 demonstrates that there was no appreciable contamination around the resonance energies due to reactions in the sample backing with amplitudes higher than channel ≈9. Therefore, signals due to $^{33}$S could be separated by a threshold at channel ≈9, which depends on the energy range. The fraction of true signals below the selected threshold has been recovered with accurate fits of the pulse height histograms as will be explained later. A possible contamination from $^{33}$S$(n,p)^{33}$P reactions could be neglected because of the very low cross-section [6].

### A. Cross-section determination

In the present work the $^{33}$S$(n,\alpha)^{30}$Si cross section has been determined relative to the $^{10}$B$(n,\alpha)^{7}$Li, a neutron cross-section standard in the energy range from 0.025 eV to 1 MeV [19]. Under the assumption of a thin target approximation the cross section can be determined with the following expression:

$$\sigma_{33}(E) = \sigma_{10}(E)\frac{C^{\alpha}_{33}(E)\varepsilon_{10}(E)N_{10}}{C^{\alpha}_{10}(E)\varepsilon_{33}(E)N_{33}}. \quad (1)$$

Here $C^{\alpha}$ is the number of counts due to $\alpha$ particles for both reactions corrected for the background, noise, and dead time; $\varepsilon$ is the efficiency of the detector for each reaction that depends on the geometry, the absorption of $\alpha$ particles in the sample,

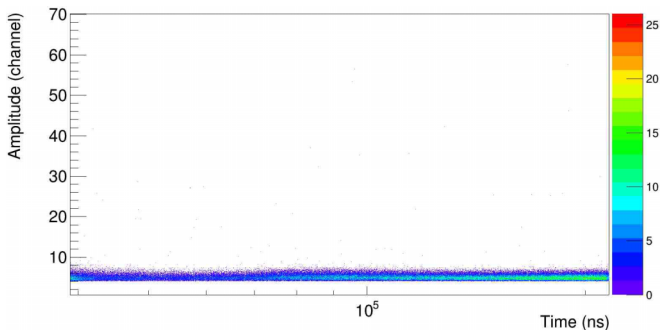


FIG. 2. Scatter plot of the signal amplitude in arbitrary units (channels) versus TOF for a blank sample (substrate of a $^{33}$S sample).

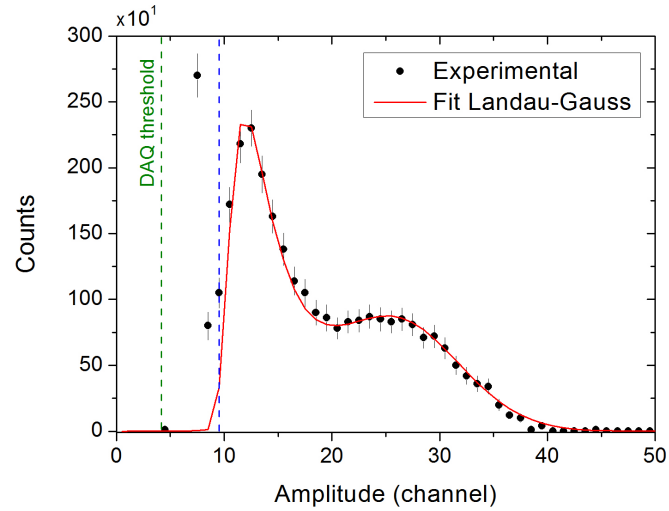


FIG. 3. Pulse height distribution of the amplitude of the signals detected in a MGAS detector. The points correspond to the experimental data with statistical uncertainties, and the red line corresponds to the fit of the distribution. The dashed blue line indicates a cut which corresponds to the cancellation of the background signals. The dashed green line indicates the selected amplitude threshold for the detector in the DAQ during the experiment.

and the kinematics of the considered reaction; and $N$ is the number of atoms per barn of $^{33}$S and $^{10}$B. In Eq. (1) it is assumed that the neutron fluence is the same for both reactions. In order to consider possible differences in the fluence seen by each sample, the transmission factors of the neutrons through all the materials (the most important are due to Kapton and aluminum windows) were taken into account in the analysis. $C^{\alpha}$ and $\varepsilon$ depend on the energy. In the conversion from TOF to energy the time-energy relation of the n_TOF beam was considered. This function includes the effects of the neutron production mechanisms and the moderation process with the configuration of the moderation-cooling system [11,20]. Before the present experiment, an accurate determination of the flight path was carried out via low-energy resonances of the $^{235}$U$(n,f)$ reaction following the method explained in Ref. [21].

The determination of the number of counts due to $\alpha$ particles and the background subtraction is illustrated in Fig. 3, which shows an experimental pulse height distribution (black points) with statistical uncertainties in one of the MGAS detectors. Several works have studied the distribution of pulse height in MGAS detectors with different gases and particles concluding that it can be described with a convolution of Landau and Gaussian functions [22,23]. Figure 3 shows an example of an experimental pulse height distribution and the fit with Landau-Gauss functions performed in the present analysis. The integration of the fit function provides the number of $\alpha$ particles in the selected energy range. Signals due to background and noise induced by the backing and the detector itself dominate the number of counts for channels below channel 10. Indeed, the point at channel 7 has a value of 2700 counts and the points at channels 5 and 6, with much higher numbers of counts, are not included for visualization purposes. Therefore,

we can conclude that the amplitude of the $\alpha$-particles signals appears from channels 0 to 50 and the amplitude of the background signals appears only at low amplitudes. The same was concluded from the comparison between Figs. 1 and 2.

The subtraction of the background has been performed by making a selection of the $\alpha$-particle signals. The vertical dashed blue line would correspond to a horizontal cut in the scatter plot of Fig. 1 at an amplitude slightly lower than channel 10, which is considered the most adequate in the selected energy range. This cut implies a loss in the number of $\alpha$ particles from 0.75 to 1.5% depending on the selected energy range, which are recovered by the integration of the fitting function from channels 0 to 50. The dashed green line corresponds to the amplitude threshold chosen for the detectors in the DAQ during the experiment. This procedure was applied in the whole energy range analyzed in the present work for all the $^{33}$S samples. For the $^{10}$B reference, the determination of the number of counts was identical to previous experiments at n_TOF with a $^{10}B_4C$ sample and a MGAS detector [12].

### B. Efficiency and dead time

The $^{33}S(n,\alpha)^{30}Si$ cross section has been determined relative to the $^{10}B(n,\alpha)^{7}Li$ measured simultaneously with the same kind of detectors housed in the same chamber and the same analysis procedure and experimental conditions. In particular, for both reactions the detected ions fully deposited their energy in the gas of the MGAS detector. Also the calculation of the loss of signals due to the subtraction of the background was considered by means of the integration of the fit function of the pulse height distributions. Therefore the correction for the detector efficiency is reduced to the absorption in the samples and the kinematics of each reaction.

Detailed Monte Carlo simulations of the energy loss, absorption, and scattering in the samples of the $\alpha$ particles from $^{33}S(n,\alpha)^{30}Si$ and $^{10}B(n,\alpha)^{7}Li$ reactions were performed by means of MCNPX [24]. It was considered that the $\alpha$ particles were uniformly distributed inside the samples. In the case of the $^{10}B_4C$ sample the angular distribution of the $\alpha$ particles of the reactions on $^{10}$B reported in Ref. [25] was taken into account. For the $^{33}S(n,\alpha)^{30}Si$ reaction, it was assumed that the $\alpha$ emission was isotropic in the center-of-mass system. The validity of this assumption was checked by means of the comparison between each pair of forward and backward $^{33}$S samples. For each pair, the same yield was obtained for the existing resonances, within uncertainties. Figure 4 shows the efficiency in the forward direction obtained for both reactions in the analyzed energy range. The increase in the efficiency of $^{10}$B MGAS is due to the forward-peaked anisotropy of the dominant channel, which produces $^{7}$Li in its first excited state, above 100 keV [25].

For the present measurement, the characteristics of the n_TOF-EAR1 facility reduce the possibility of dead-time and pile-up problems. However, the intrinsic width of the MGAS signals (250 ns) could produce a remaining very small dead-time effect. Nevertheless, in the energy range analyzed in the present experiment no significant dead time was found even for the $^{10}B(n,\alpha)^{7}Li$ reaction, as in other experiments performed at the n_TOF-EAR1 facility [12].

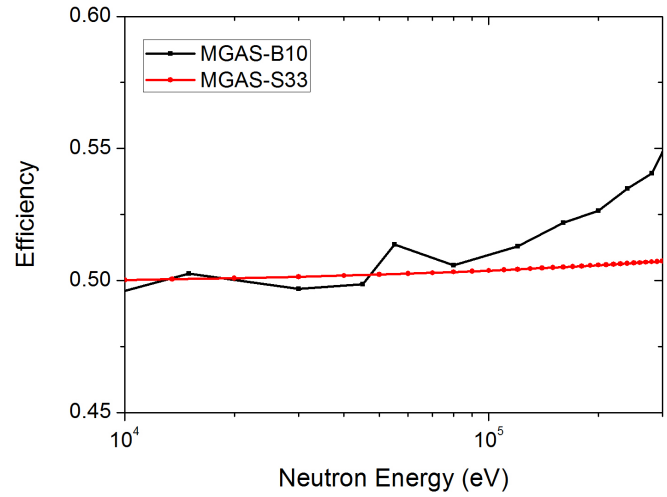


FIG. 4. Simulated efficiency for the detection of $\alpha$ particles emitted in the forward direction with the MGAS detector configuration in the present experiment.

### C. Uncertainty

Here, the main sources of uncertainty and their relevance are discussed with the aim of providing a conservative estimation of the accuracy of the present results. The major sources of uncertainty were the masses of the $^{33}$S samples and the statistical uncertainty of the data. As discussed in Ref. [15], ≈9% relative uncertainty was obtained including the small inhomogeneities in the mass distribution. Concerning the normalization to the standard $^{10}B(n,\alpha)^{7}Li$ reaction, the uncertainty in the cross section is lower than 1% below 180 keV [19]. The uncertainties related to the angular emission of the $\alpha$ particles of the $^{10}B(n,\alpha)^{7}Li$ reaction can be neglected because of the large angle covered by the MGAS detector and the accurate angular distributions reported in Ref. [25]. Therefore, we assume an overall contribution of 4% due to the normalization to the standard cross-section and the uncertainties related to the $^{10}B_4C$ sample.

Another uncertainty component is caused by the detection efficiency, which depends on the energy. The statistical uncertainty in the simulations of the $\alpha$-particle transport, discussed in Sec. III B, was lower than 1%. The selected threshold for the detectors and the cuts in the histograms of signal amplitude supposed a signal loss, already discussed in Sec. III A. The total number of signals due to $\alpha$ particles for both reactions were determined by fitting the pulse height distributions of the $\alpha$-induced signals from channels 0 to 50. It is shown in Fig. 3 that good fits can be achieved within the limits of the statistical accuracy of the experimental data; for this reason a 3% uncertainty in the fits has been assumed as a conservative estimation. The uncertainties due to the neutron beam attenuation or scattering in the aluminum windows of the n_TOF tube, the Kapton windows of the MGAS chamber, the MGAS detectors and the stack of samples are 1% [12]. The present experiment was performed with six $^{33}$S samples to decrease the statistical uncertainty of the final result. Table II summarizes the sources of uncertainty.

TABLE II. Major sources of uncertainty (in %) of the present $^{33}S(n,\alpha)^{30}Si$ cross section. The statistical uncertainty of the number of counts ranges from 8−35% depending on the energy range (resonances and valleys).

| Component | Uncertainty (%) |
|---|---|
| Sample mass $^{33}S$ | 8–9 |
| Statistical uncertainty $^{33}S$ | 8–35 |
| Normalization and $^{10}B_4C$ sample | 4 |
| Pulse height fit | 3 |
| Neutron beam attenuation | 1 |

The results of the analysis are shown and discussed in Sec. IV. The pointwise cross section from 10 to 300 keV will be uploaded into the EXFOR database [26].

## IV. RESULTS

This experiment aimed at reducing possible sources of uncertainties and to improve some issues related to the setup and the analysis of previous measurements [6,9]. In the energy range from 10 to 200 keV, previous $(n,\alpha)$ measurements used as reference the $^{235}U(n,f)$ cross section [6,9], which for neutron energies below 100 keV was standard only at thermal energy. In both experiments, the reference cross section was not measured simultaneously with $^{33}S(n,\alpha)^{30}Si$. Regarding the samples, Wagemans *et al.* reported important problems due to the sulfur loss in a previous experiment that were solved by sealing the sample in a formvar-sulfur-formvar sandwich [13]. However, the mass of the sample was not measured after the experiment. The reported masses were based on the combination of the count rate under irradiation with a thermal neutron beam, a nondestructive analysis, and a destructive chemical analysis resulting in a mass uncertainty larger than 20% [13]. Also Auchampaugh *et al.* reported sulfur losses during their experiment. A loss of one-third of the mass of the sample was determined in a reactor a few days after the experiment, making use of a thermal value of $(140 \pm 30)$ mb for the $^{33}S(n,\alpha)^{30}Si$ cross section [9]. Wagemans *et al.* [6] also used the thermal point, with a value of $(115 \pm 10)$ mb, for obtaining the integrated area of the 13.45-keV resonance in a measurement with low-energy resolution (short flight path). Then, the final measurement, carried out using a longer flight path, was normalized to the integrated area of the 13.45-keV resonance obtained with the shorter flight path [6].

Some improvements in the present experiment are related to the use of the $^{10}B(n,\alpha)^{7}Li$ cross section as the unique normalization, which is a neutron standard in the whole measured energy range. Moreover, the $^{33}S(n,\alpha)^{30}Si$ and $^{10}B(n,\alpha)^{7}Li$ cross sections were simultaneously measured with the same setup. In addition, the $^{33}S$ samples were carefully characterized before and after the experiment for checking their stability [15]. The $^{33}S(n,\alpha)^{30}S$ thermal cross section, which has scattered values, was not been used.

Figure 5, left $Y$ axis, shows the $^{33}S(n,\alpha)^{30}Si$ experimental data obtained at n_TOF (black points) with Eq. (1). They are named "Yield/(Areal Density) Broadened" instead of cross section to emphasize they are still affected by the multiple scattering, Doppler broadening, self-shielding, and resolution function of the facility at EAR1. Figure 5, left $Y$ axis, also shows the n_TOF $R$-matrix fit of the experimental data (red line), which is discussed in Sec. V. Figure 5, right $Y$ axis, shows the cross section at 300 K reconstructed from the resonance parameters obtained with the n_TOF $R$-matrix fit (see Sec. V and Table III).

From 10 to 300 keV, 11 resonant structures have been found, which are also present in Wagemans *et al.* data [6] (we refer to it as Geel following the nomenclature in Refs. [5] and [6]). The analysis performed in Ref. [6], which was combined with the analysis of Coddens *et al.* [5] (we refer it as ORNL following the nomenclature in Refs. [5] and [6]) allowed the association of these structures with a total number of 14 $(n,\alpha)$ resonances. The n_TOF analysis has provided the same resonances with some differences that are briefly discussed in the next paragraph. With regard to other $(n,\alpha)$ measurements, Auchampaugh *et al.* [9] measured the $(n,\gamma)$ and $(n,\alpha)$ cross sections but they did not resolve the $(n,\alpha)$ resonances. Koehler *et al.* [27] resolved some resonances at LANSCE in an experiment with the aim of characterizing a detector based on ZnS but the energy resolution was lower than Wagemans *et al.* [6].

An important motivation of the present experiment was to study the first known resonance, at a neutron energy of 13.45 keV, due to the different description in terms of resonance parameters provided by ORNL and Geel, although they combined and shared their data and analysis [5,6]. The n_TOF data show a stronger resonance than Geel in EXFOR [26], specifically, the integrated area from 12.5 to 14.5 keV is a factor 1.5 times that of Geel. As is be shown in Sec. V, consistently the n_TOF parametrization does not agree with Geel and does agree with ORNL for this resonance.

For the remaining resonances, the same value of the integrated area as Geel within uncertainties has been obtained except for those at 70.86 and 127.66 keV. The n_TOF resonance at 70.86 keV shows a 1.8 times higher value of the integrated area compared to the Geel value. However, it should be stressed that close to the 70.86-keV resonance in the Geel data there is a resonance at 67.8 keV [6,26], which does not appear in our data in the capture measurement of Auchampaugh *et al.* [9], or in the ORNL transmission measurement [5]. In fact, the structure at 67.8 keV was not included as a resonance in the combined analysis carried out by ORNL and Geel [5,6]. For the resonance at 127.66 keV, a factor 1.9 times that of the Geel value of the integrated area has been found.

## V. *R*-MATRIX ANALYSIS

As mentioned before, the transmission experiment at ORNL and the $(n,\alpha)$ experiment at Geel combined their data for determining the resonance parameters $(E, J^{\pi}, \Gamma_n, \Gamma_{\alpha})$ up to 270 keV. The $\Gamma_{\gamma}$ values were obtained by ORNL from the capture measurement of Auchampaugh *et al.* [9]. In the ORNL analysis the determination of $J^{\pi}$ of each resonance was explained in detail and was assumed in the present analysis. The Bayesian code SAMMY [7] in the Reich-Moore approximation of the $R$-matrix theory was used for the analysis. As discussed in Sec. III, the background was subtracted by means of cuts in

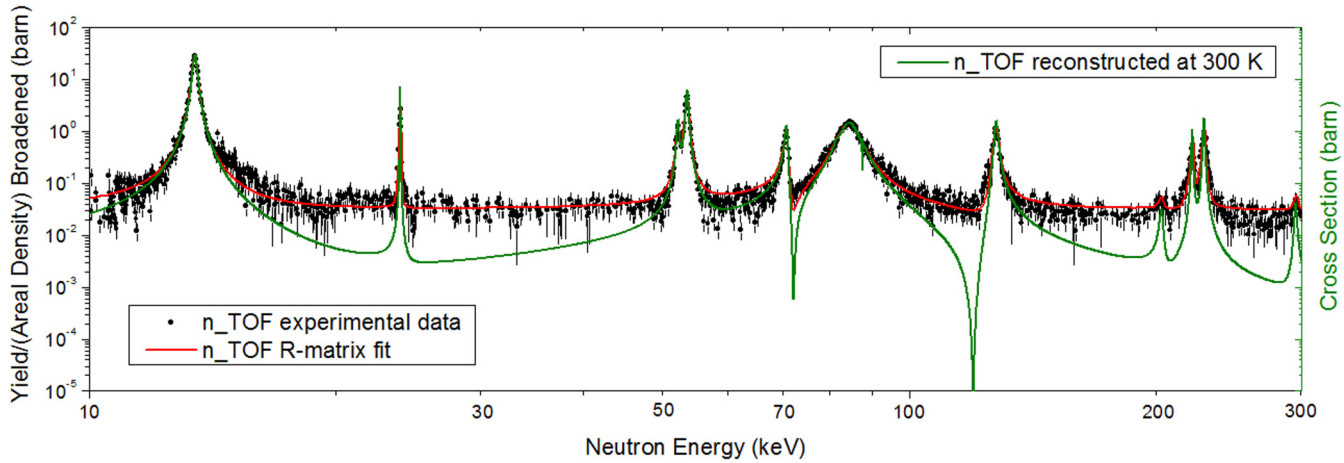


FIG. 5. Left $Y$ axis: Experimental data of the $^{33}$S$(n,\alpha)$ $^{30}$Si reaction measured at n_TOF (black points) and the fit performed in Sec. V (red line) in the energy range from 10 to 300 keV. Both are affected by the multiple scattering, Doppler broadening, self-shielding, and resolution function of the facility at EAR1. Right $Y$ axis: $^{33}$S$(n,\alpha)$ $^{30}$Si cross section at 300 K reconstructed from the resonance parameters obtained in the analysis performed in Sec. V, only affected by Doppler broadening.

the amplitude histograms that were adjusted for each energy range. Then, accurate fits of the amplitude histograms were performed for recovering the $\alpha$-induced signal losses due to the cuts. However, a better fit of the valleys between resonances was achieved if a small constant background of 20 mb was included in the SAMMY fit. The n_TOF experimental data or yield/(areal density) broadened data, red points in Figs. 6 to 9, were fitted considering only statistical uncertainties. As mentioned in Sec. IV, the experimental data are affected by Doppler broadening, multiple scattering, self-shielding, and resolution function. All these effects were included in the fit with SAMMY for every set of parameters (ORNL, Geel, and n_TOF). The normalization was fixed to 1.0. The potential scattering was taken into account using a radius of 3.85 fm [5].

The procedure we followed was to describe the n_TOF data from 10 to 300 keV with the resonance parameters of ORNL and/or Geel. When this was not possible $\Gamma_\alpha$ was adjusted as a free parameter. In this way, the experimental data

TABLE III. Resonance parameters and $\alpha$ strength ($g\Gamma_n\Gamma_\alpha/\Gamma$) of the $^{33}$S$(n,\alpha)$ $^{30}$Si resonances obtained in the present work (n_TOF), in the transmission experiment (ORNL) of Coddens *et al.* [5], and in the $(n,\alpha)$ measurement (Geel) of Wagemans *et al.* [6]. An empty space means the same value as Geel and the symbol "—" means that the resonance was not detected or studied (see text for details). The quoted uncertainties of the new values provided in our analysis were obtained by the SAMMY fit. For $\Gamma_\gamma$ and $\Gamma_n$ the uncertainty provided in Ref. [5] was assumed except those indicated with a superscript d.

| $E_n$ (keV) | $J^\pi$ [a] | $\Gamma_\gamma$ [b] (eV) | $\Gamma_n$ [c] (eV) | $\Gamma_\alpha$ (eV) | | | $g\Gamma_n\Gamma_\alpha/\Gamma$ (eV) | | |
|---|---|---|---|---|---|---|---|---|---|
| | | | | n_TOF | ORNL | Geel | n_TOF | ORNL | Geel |
| 13.45 | $2^+$ | 0.25 ± 0.05 | 75 ± 1 | 100 ± 5 | 83 ± 3 | 41 ± 5 | 27.0 ± 0.4 | 24.6 ± 0.5 | 16.4 ± 1.1 |
| 23.95 | $3^-$ | 1.45 ± 0.10 | 16.0 ± 0.9 | 2.2 ± 0.4 | | 2.5 ± 0.3 | 1.57 ± 0.09 | | 1.86 ± 0.16 |
| 52.12 | $2^+$ | 0.25 ± 0.05 | 349 ± 6 | | | 18 ± 2 | | | 10.5 ± 1.2 |
| 53.60 | $3^-$ | 1.6 ± 0.3 | 68 ± 3 | 320 ± 10 | 120 ± 11 | 83 ± 13 | 47 ± 3 | 38 ± 2 | 32.6 ± 2.0 |
| 70.86 | $1^-$ | 0.68 ± 0.15 | 65 ± 10 | 580 ± 20 | 170 ± 50 | 107 ± 63 | 22 ± 4 | 18 ± 3 | 15.1 ± 1.9 |
| 81.36 | $2^+$ | 0.95 ± 0.06 | 705 ± 19 | | | 4 ± 2 | | | 2.5 ± 1.2 |
| 84.88 | $1^-$ | 0.8 ± 0.09 | 720 ± 25 [d] | 4500 ± 100 | 3900 ± 300 | 3970 ± 600 | 232 ± 8 | 370 ± 20 | 374 ± 24 |
| 87.63 | $1^-$ | 2.14 ± 0.14 | 28 ± 5 [d] | 1 ± 0.2 | | 10 ± 5 | 0.34 ± 0.06 | | 3.6 ± 1.8 |
| 127.66 | $1^-$ | 1.7 ± 0.4 | 360 ± 40 | 950 ± 110 | 520 ± 120 | 127 ± 60 | 98 ± 11 | 80 ± 11 | 58 ± 6 |
| 203.32 | $3^-$ | 2.2 ± 0.2 | 2090 ± 42 | 5 ± 2 | | 14 ± 5 | 4.4 ± 0.09 | | 12 ± 4 |
| 221.38 | $2^+$ | 1.4 ± 0.4 | 690 ± 70 | 140 ± 14 | 280 ± 100 | 55 ± 20 | 73 ± 8 | 120 ± 30 | 32 ± 14 |
| 223.17 | $0^+$ | 0.68 ± 0.12 | 4400 ± 900 | | | 900 ± 300 | | | 93 ± 25 |
| 228.73 | $3^-$ | 0.84 ± 0.13 | 760 ± 50 | 230 ± 30 | 230 ± 60 | 203 ± 27 | 150 ± 11 | 150 ± 30 | 140 ± 14 |
| 295.95 | $2^+$ | 2.2 ± 0.15 | 2090 ± 100 | 15 ± 5 | — | — | 9.3 ± 0.5 | — | 42 ± 10 |

[a]Determined by ORNL except 295.95 keV, which is tentative (see text for details).
[b]Determined by ORNL from the $(n,\gamma)$ data of Auchampaugh *et al.* [9].
[c]Determined by ORNL except where it is indicated (see text for details).
[d]$\Gamma_n$ ORNL values: 1330 ± 80 eV for 84.88 keV and 280 ± 20 eV for 87.63 keV.

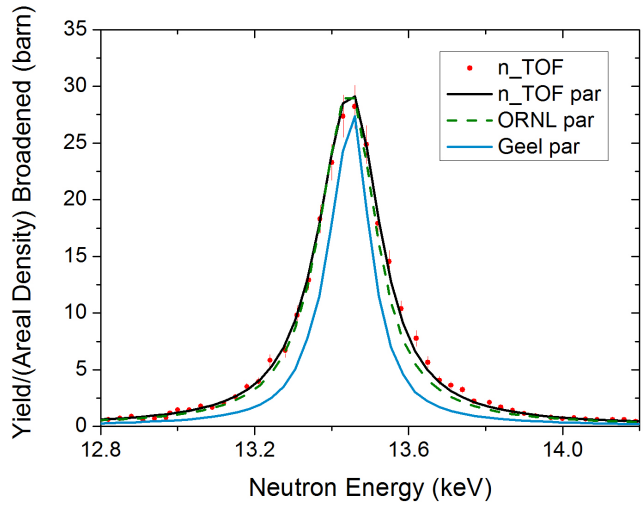


FIG. 6. *R*-matrix analysis from 12.8 to 14.2 keV. The n_TOF data (red points) are compared with the description of ORNL [5] (dashed green line), Geel [6] (blue line), and the present work (black line).

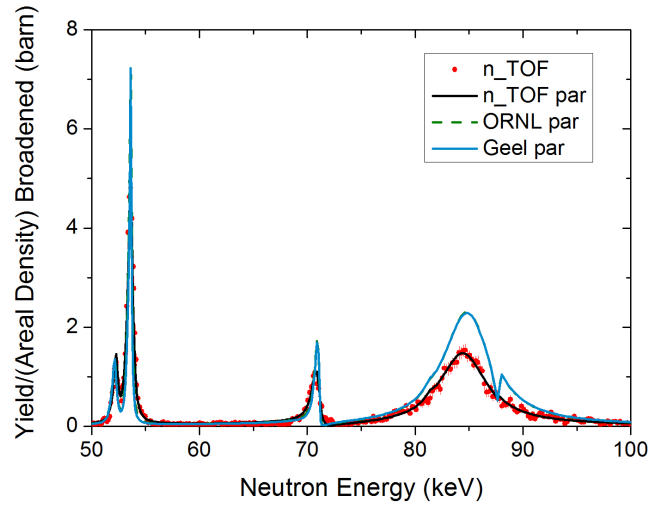


FIG. 7. *R*-matrix analysis from 50 to 100 keV. The n_TOF data (red points) are compared with the description of ORNL [5] (dashed green line), Geel [6] (blue line), and the present work (black line). Geel and ORNL are coincident from 60 to 100 keV.

were consistently described for the resonant structure from 75 to 100 keV, which was needed to change the $\Gamma_n$ values, as discussed later. In the following, the n_TOF analysis is discussed and compared with Coddens *et al.* [5] (ORNL) and Wagemans *et al.* [6] (Geel). It is split in four figures throughout this section only for visualization purposes and justification of the new parameters found for a few resonances.

Table III shows the resonance parameters and $\alpha$ strengths obtained in the present work (n_TOF), in comparison with ORNL and Geel. The $\alpha$ strength is defined as $g\Gamma_n\Gamma_\alpha/\Gamma$, where $\Gamma = \Gamma_n + \Gamma_\alpha + \Gamma_\gamma$ is the total width; $g = (2J+1)/[(2I+1)(2i+1)]$ is the statistical factor and $J$, $I$, and $i$ are the spins of the resonance, the target ($\frac{3^+}{2}$), and the projectile, respectively. Because ORNL and Geel combined their data, many of the $\Gamma_\alpha$ values and strengths were identical. This was highlighted in their tables by an empty space reserved for the parameter of the corresponding resonance [5,6]. We follow their nomenclature see Table III, in which an empty space means the same value as Geel and "—" means that the resonance parameter is not available because the resonance was not detected or because the parameter could not be determined.

The study of the 13.45-keV resonance is an important goal due to the discrepant descriptions obtained by ORNL and Geel, specifically ORNL provided a value of $\Gamma_\alpha$ twice the one of Geel (see Table III). For this resonance a value of the integrated area higher than Geel has been obtained, as mentioned in Sec. IV, therefore, it is expected that the n_TOF data would provide a higher value of the strength too. Figure 6 shows the 13.45-keV resonance in which the n_TOF data (red points) are compared with the resonance parametrizations carried out by ORNL (dashed green line), Geel (blue line), and the present work (black line). An excellent description is obtained with the $\Gamma_\alpha$ value of n_TOF (see Table III). Nevertheless, n_TOF data are fitted within statistical uncertainties with the $\Gamma_\alpha$ value of ORNL, which is not possible with the $\Gamma_\alpha$ value of Geel. This consolidates the n_TOF description of the resonance and suggests that the Geel analysis underestimated its strength.

Figure 7 shows the energy range from 50 to 100 keV. As was mentioned, the same value of the area of the resonance at 53.6 keV as Geel was obtained. However, the fit of the resonance is not possible, neither with the $\Gamma_\alpha$ value of Geel nor with the ORNL value. For this reason, although the area is the same, the n_TOF analysis provides a new value of $\Gamma_\alpha$ (see Table III). The resonance at 70.86 keV showed a higher area than Geel and, indeed, the $\Gamma_\alpha$ value of n_TOF is also higher. For both resonances, the n_TOF strength is slightly higher than that of ORNL and Geel.

The structure from 75 to 100 keV was described by ORNL and Geel as three resonances at 81.36, 84.88, and 87.63 keV. The parametrization of ORNL and Geel does not fit the n_TOF data, providing an overestimation of the cross section compared to our data. We tried to fit the n_TOF data leaving free only $\Gamma_\alpha$ but it was not possible. To fit this structure it was needed to change the $\Gamma_n$ parameters provided by ORNL. In fact, the key point was reducing the $\Gamma_n$ values of ORNL for the 84.88- and 87.63-keV resonances. This reduction is justified because the $\Gamma_n$ values were obtained in the ORNL analysis considering a full interference between both resonances but a partial interference is also acceptable, which provides a different value of $\Gamma_n$, as discussed in Ref. [5]. In consequence, we propose to describe the resonant structure from 75 to 100 keV as the three resonances proposed by ORNL and Geel with the parameters of Table III. The strength of the resonances at 84.88 and 87.63 keV obtained by n_TOF is significantly lower than that of ORNL and Geel, while the resonance at 81.36 keV remains identical to the analysis of ORNL and Geel.

Figure 8 shows the energy range from 124 to 132 keV for which a resonance with a larger area than Geel was found, as mentioned in Sec. IV. The parametrization of ORNL is close to the n_TOF data while the set of parameters of Geel underestimated the resonance. Nevertheless, we provide a better description of the 127.66-keV resonance (black line in Fig. 8) by changing only $\Gamma_\alpha$. The obtained strength is much

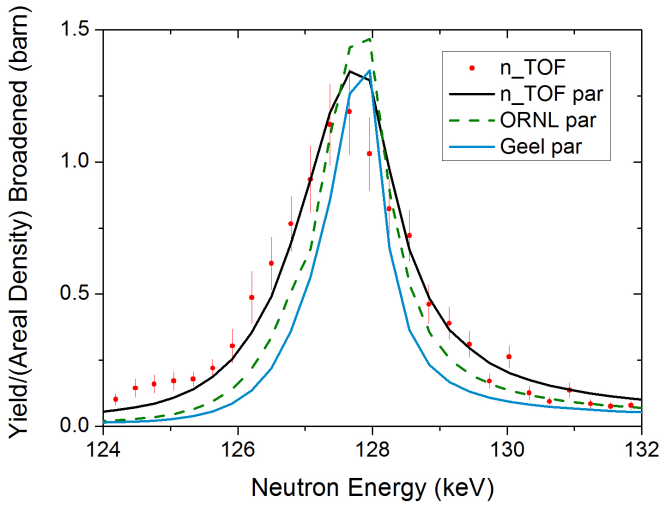


FIG. 8. *R*-matrix analysis from 124 to 132 keV. The n_TOF data (red points) are compared with the description of ORNL [5] (dashed green line), Geel [6] (blue line), and the present work (black line).

higher than that of Geel and matches within uncertainties the that of ORNL (see Table III).

Figure 9 shows the energy range from 200 to 240 keV. With regards to the 221.38-keV resonance, the n_TOF parametrization provides a $\Gamma_\alpha$ value higher than that of Geel but lower than that of ORNL, consistent with the significant overestimation of the resonance by ORNL (see the dashed green line). Concerning the 228.6-keV resonance, our data are described with the parameters of ORNL; nevertheless the $\Gamma_\alpha$ value and strength match the Geel values within uncertainties.

Finally, to complete the analysis up to 300 keV, a very small structure at 296.2 keV was described as a resonance in the Geel analysis. At this energy also a $(n,\gamma)$ resonance was resolved by Auchampaugh *et al.* [9]. Due to the fact that the ORNL and Geel analyses did not provide resonance parameters we have described it with a tentative $J^\pi$ value and reasonable values of the resonance parameters in comparison with the 203.32-keV resonance (see Table III and Fig. 5).

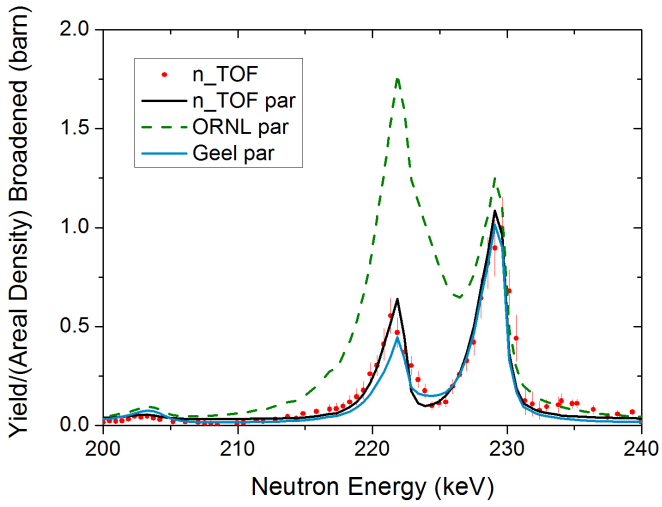


FIG. 9. *R*-matrix analysis from 200 to 240 keV. The n_TOF data (red points) are compared with the description of ORNL [5] (dashed green line), Geel [6] (blue line), and the present work (black line).

## VI. $^{33}$S $(n,\alpha)$ IN BNCT AND ASTROPHYSICS

One of the aims of this work was to measure and characterize the 13.45-keV resonance because of its possible contribution to the dose in neutron-capture therapy with epithermal neutron beams and tumors with uptake of $^{33}$S [1,3,4]. We have found that the integrated area from 12.5 to 14.5 keV is a factor 1.5 times higher than the Geel value [6]. The value of $\Gamma_\alpha$ in our parametrization is in agreement with the ORNL value, which was twice that of Geel. Accordingly, n_TOF data will provide higher values of the delivered dose than obtained in Refs. [1,3,4], which used the Geel data. This would imply a higher destruction of the tumor for the same neutron fluence and $^{33}$S uptake. However, to carry out more realistic simulations of the dose in tissue, we need to measure the cross section from thermal values to 10 keV. At thermal energy few data exist and they disagree by more than 30%, whereas from thermal values to 10 keV there are no data at all.

In addition, more factors have to be taken into account in the determination of the dose, for instance, the biological effect of the $^{33}$S$(n,\alpha)$ $^{30}$Si reaction could be higher than that of the $^{10}$B$(n,\alpha)$ $^{7}$Li reaction due to the higher $Q$ value. Also, the biological effect depends on the carrier, which for $^{33}$S is under investigation. All of these are matters of research at present [28]. From the nuclear physics side, the present n_TOF data encourage the continuation of research on $^{33}$S as a target in BNCT.

Regarding astrophysics, the role of $^{33}$S for the origin of $^{36}$S in explosive scenarios was studied by Wagemans *et al.* [6] and Auchampaugh *et al.* [9], showing an overproduction in the solar system incompatible with the stellar models. The Maxwellian-average cross section (MACS) at different $kT$ was calculated without experimental data from thermal values to 10 keV. In addition, Wagemans *et al.* [6] and Auchampaugh *et al.* [9] used thermal values that disagreed by more than 20%. As demonstrated by Druyts *et al*. [29], the thermal value has a direct impact on the MACS values. Therefore, to obtain more accurate MACS, experimental data from thermal values to 10 keV are necessary for concluding on the role of $^{33}$S in explosive scenarios.

## VII. SUMMARY

The $^{33}$S$(n,\alpha)$ $^{30}$Si cross section has been measured at the EAR1 of the n_TOF facility at CERN relative to the standard $^{10}$B$(n,\alpha)$ $^{7}$Li cross section covering the energy range from 10 to 300 keV. Both reactions were measured simultaneously with the same setup. With the 185-m flight path and the experimental setup based on MGAS detectors it has been possible to achieve a high-resolution measurement in neutron energy and good discrimination between $\alpha$ particles and background. Monte Carlo simulations of the detector efficiency and accurate fits of the amplitude histograms have been performed to correct for $\alpha$-particle losses. Eleven resonancelike structures have been resolved. For three of them (13.45, 70.86, and 127.66 keV), a value of the area higher than the unique available high-resolution $(n,\alpha)$ measurement [6] was found.

A detailed resonance analysis in the Reich-Moore approximation of the $R$-matrix theory has been performed using the SAMMY code. New $\Gamma_\alpha$ values and strengths have been provided for some of the resonances after a detailed discussion. The $R$-matrix analysis showed that the 11 resonant structures can be associated with 14 individual resonances, the same as ORNL and Geel. The cross section at 300 K has been provided by means of its reconstruction from the resonance parameters obtained in the present $R$-matrix analysis. Of special interest is the most important resonance at 13.45 keV, which has been consistently described with the ORNL transmission data [5], but was found to disagree significantly from with the $(n,\alpha)$ result obtained at Geel [6].

The present data could promote new evaluations of the cross section in view of the important discrepancies between present evaluated libraries's evaluations and the available experimental data.

## ACKNOWLEDGMENTS

This work was supported by the Spanish projects FPA2013-47327-C2-1-R, FPA2016-77689-C2-1-R, J. de Andalucía P11-FQM-8229, and FIS2015-69941-C2-1-P (MINECO-FEDER, EU); the Spanish Association Against Cancer (AECC) (Grant No. PS16163811PORR); and the funding agencies of the participating institutes.

[1] I. Porras, Phys. Med. Biol. **53**, L1 (2008).
[2] Nuclear Physics European Collaboration Committee, *Nuclear Physics for Medicine*, http://www.nupecc.org/.
[3] I. Porras, Appl. Radiat. Isot. **69**, 1838 (2011).
[4] J. Praena, M. Sabaté-Gilarte, I. Porras, P. L. Esquinas, J. M. Quesada, and P. Mastinu, Appl. Radiat. Isot. **88**, 203 (2014).
[5] G. P. Coddens, M. Salah, J. A. Harvey, N. W. Hill, and N. M. Larson, Nucl. Phys. A **469**, 480 (1987).
[6] C. Wagemans, H. Weigmann, and R. Barthelemy, Nucl. Phys. A **469**, 497 (1987).
[7] N. M. Larson, Updated Users Guide for SAMMY: Multilevel R-matrix Fits to Neutron Data Using Bayes Equations, SAMMY, Computer Code, Report No. ORNL/TM-9179/R7, Oak Ridge National Laboratory, 2008.
[8] The Evaluated Nuclear Reaction Databases, https://www-nds.iaea.org/exfor/endf.htm.
[9] G. F. Auchampaugh, J. Halperin, R. L. Macklin, and W. M. Howard, Phys. Rev. C **12**, 1126 (1975).
[10] R. Reifarth, K. Schwarz, and F. Käppeler, Astrophys. J. **528**, 573 (2000).
[11] C. Guerrero, A. Tsinganis *et al.* (n_TOF Collaboration), Eur. Phys. J. A **49**, 27 (2013).
[12] M. Barbagallo, C. Guerrero *et al.* (n_TOF Collaboration), Eur. Phys. J. A **49**, 156 (2013).
[13] K. Geerts, J. van Gestel, and J. Pauwels, Nuc. Instrum. Methods Phys. Res., Sect. A **236**, 527 (1985).
[14] J. García López, F. J. Ager, M. Barbadillo Rank, F. J. Madrigal, M. A. Ontalba, M. A. Respaldiza, and M. D. Ynsa, Nucl. Instrum. Methods Phys. Res., Sect. B **161-163**, 1137 (2000).
[15] J. Praena, F. J. Ferrer, W. Vollenberg *et al.* (n_TOF Collaboration), Nucl. Instrum. Methods Phys. Res., Sect. A **890**, 142 (2018).
[16] G. Charpak, Y. Giomataris, J. Derr, and Ph. Rebourgeard, Nucl. Instrum. Methods Phys. Res., Sect. A **478**, 26 (2002).
[17] S. Andriamonje *et al.*, J. Korean Phys. Soc. **59**, 1597 (2011).
[18] U. Abbondanno *et al.* (n_TOF Collaboration), Nucl. Instrum. Methods Phys. Res., Sect. A **538**, 692 (2005).
[19] A. D. Carlson *et al.*, Nucl. Data Sheets **110**, 3215 (2009).
[20] G. Lorusso *et al.* (n_TOF Collaboration), Nucl. Instrum. Methods Phys. Res., Sect. A **532**, 622 (2004).
[21] M. Calviani, J. Praena *et al.* (n_TOF Collaboration), Phys. Rev. C **80**, 044604 (2009).
[22] Y. Giomataris, R. De Oliveira *et al.*, Nucl. Instrum. Methods Phys. Res., Sect. A **560**, 405 (2006).
[23] C. Bernet, J. Abbon, J. Ball *et al.*, Nucl. Instrum. Methods Phys. Res., Sect. A **536**, 61 (2005).
[24] D. B. Pelowitz, MCNPX Users Manual, Version 2.5.0, LA-CP05-0369, Los Alamos National Laboratory LACP, 2005.
[25] F. J. Hambsch and I. Ruskov, Nucl. Sci. Eng. **163**, 1 (2009).
[26] N. Otuka *et al.*, Nucl. Data Sheets **120**, 272 (2014).
[27] P. E. Koehler, J. A. Harvey, and N. W. Hill, Nucl. Instrum. Methods Phys. Res., Sect. A **361**, 270 (1995).
[28] I. Porras, M. C. Ruiz, M. Pedrosa, F. Arias de Saavedra, M. J. Ruiz, and J. Praena, Determination of Relative Biological Effectiveness for BNCT by Irradiation of Cell Cultures, ILL Research Proposal 75329, 2016.
[29] S. Druyts, C. Wagemans, and P. Geltenbort, Nucl. Phys. A **537**, 291 (1994).